Scope of work

MASTER THESIS 2014

for

Stud. techn. Heidi Jacobsen

Structural design considerations for an ice resistance semi-submersible drilling rig

Strukturdesign for en isforsterket halvt nedsenkbar borerigg

With large prospects of oil and gas field development in the Arctic and sub-Arctic areas, there is a current market demand for robust drilling and field development solutions. The Arctic areas are characterized by long distances, harsh weather conditions and the possibility for ice encounters, both from level ice and icebergs. Drilling while surrounded by ice can be difficult due to the stringent station keeping demands from the drilling operation. In ice-covered regions, drilling operations are thus currently only possible during the short summer season of a few months, with low or no ice coverage. Commercial drilling operations are planned in among others the Beaufort, Barents and Kara seas.

Currently there is a severe shortage of ice-capable drilling units, and conventional units are being modified to deal with the cold temperature and light ice conditions. Due to the short drilling season, new builds with high ice capability can give significant financial risk, and few units are thus constructed.

With existing winterized drilling rigs without significant ice reinforcement, drilling will only take place in open water. With the high costs involved, field operators are expected to extend the season to complete as many wells as safely possible. This leaves the platform at risk of not making a clean exit from the location without interacting with ice. As a risk based decision tool, further knowledge of the actual (ultimate) structural capacity to ice encounters is needed.

The purpose of this project is to review the drilling concepts currently used and planned for use in Arctic areas, and investigate the actual capacity of a typical structure towards impacts from isolated ice floes. Plastic methods should be utilized to establish a framework for hand calculation methods of the interaction between the ice floe and plating, stiffeners and frames in the platform. The harsh environment ultra-deep water Moss Maritime drilling rig design CS60 will be utilized as a base case, and the actual capacity of the hull vs. the size of ice floe and impact speed should be established. Possible modifications of the structure to increase the ice resistance should be investigated and evaluated in terms of the increased structural weight.

The work may be carried out in the following steps:

1. Review of the ice design requirements to semi submersibles in transit condition given in DNV-OS-C103

2. Describe the structural configuration of the CS60 platform pontoon and columns

3. Review of the governing criteria for design of pontoons and columns in the ice exposed areas and adjacent regions. Compare the loads and structural resistance formulations applied in the design and those given for ice actions in DNV-OS-C103

4. Determine relevant ice load scenarios during transit and evaluate various alternatives for modeling and analysis of these scenarios. Consider especially whether continuum mechanics modeling of ice for ice floe impacts shall be conducted. The effect of impact geometry, speed of the two bodies and impact location shall be evaluated.

5. Establish finite element models for ice exposed structures for CS60 platform as is. Due considerations shall be given to modeling of boundary conditions and the functional load effects.

6. Perform nonlinear finite element analysis of the modeled structural components. The ice loads shall be increased so as to produce structural deformations well into the plastic domain. To the extent possible the ice loads shall be compared with the loads constituting the basis for the DNV-OS-C103 requirements, taking into account possible implicit safety factor and simplifications in the resistance formulations. The damage that will be imposed by the ice actions assumed in DNV-OS-C103 shall be predicted. Whether these damages are acceptable from a safety and economic point of view shall be discussed. The expected repair costs shall be estimated based on probability considerations of encountering severe ice conditions.

7. Investigate whether the CS60 platform structure as is can be strengthened so as to comply with the DNV-OS-C103 requirements. Estimate the costs of strengthening and compare with those of expected repair costs with no ice reinforcement actions.

8. To the extent possible results from finite element analyses shall be compared with simplified resistance formulations (refer Project thesis)

9. Conclusions and recommendations for further work

Literature studies of specific topics relevant to the thesis work may be included.

The work scope may prove to be larger than initially anticipated. Subject to approval from the supervisors, topics may be deleted from the list above or reduced in extent.

In the thesis the candidate shall present his personal contribution to the resolution of problems within the scope of the thesis work.

Theories and conclusions should be based on mathematical derivations and/or logic reasoning identifying the various steps in the deduction.

The candidate should utilize the existing possibilities for obtaining relevant literature.

Thesis format

The thesis should be organized in a rational manner to give a clear exposition of results, assessments, and conclusions. The text should be brief and to the point, with a clear language. Telegraphic language should be avoided.

The thesis shall contain the following elements: A text defining the scope, preface, list of contents, summary, main body of thesis, conclusions with recommendations for further work, list of symbols and acronyms, references and (optional) appendices. All figures, tables and equations shall be numerated.

The supervisors may require that the candidate, in an early stage of the work, presents a written plan for the completion of the work. The plan should include a budget for the use of computer and laboratory resources which will be charged to the department. Overruns shall be reported to the supervisors.

The original contribution of the candidate and material taken from other sources shall be clearly defined. Work from other sources shall be properly referenced using an acknowledged referencing system.

The report shall be submitted in two copies:

- Signed by the candidate
- The text defining the scope included
- In bound volume(s)
- Drawings and/or computer prints which cannot be bound should be organized in a separate folder
- The report shall also be submitted in PDF format along with essential input files for computer analysis, spreadsheets, Matlab files etc in digital format.

Ownership

NTNU has according to the present rules the ownership of the thesis. Any use of the thesis has to be approved by NTNU (or external partner when this applies). The department has the right to use the thesis as if the work was carried out by a NTNU employee, if nothing else has been agreed in advance.

Moss Maritime designs will be utilized in the thesis work. With the intention of allowing the results of the thesis work publicly available, Moss Maritime reserves the right to ensure that commercially sensitive information is not included in the

public part of the thesis. If such issues should arise, confidential information is suggested to be included as an appendix which is omitted from the openly available thesis.

Thesis supervisors

Prof. Jørgen Amdahl
Ph.D. student Martin Storheim
Contact person at Moss Maritime: Erik Pettersen

Deadline

June 10, 2014

Trondheim, January 14, 2014

Jørgen Amdahl

Preface

This report is the result of the Master thesis conducted by stud. techn. Heidi Jacobsen at the Norwegian University of Science and Technology, NTNU, spring 2014. The work is a continuation of the Project thesis work carried out in fall 2013. The basic theory for the problems to be addressed was reviewed, and this theory is therefore not given in the Master thesis. The work has been challenging regarding both modelling, collision setup and evaluation of the results, but the overview of ice-induced impact on such a structure has been a great motivation for me during the work.

A major part of the thesis was to establish a FE model to use in the analyses. My knowledge in FE modelling software was limited, and the time spent on modelling turned out significantly larger than anticipated. Several modelling techniques were assessed to obtain a sufficient geometry, and the combination of geometry and applied mesh created challenges for the further work. After a lot of different unsuccessful tests on the FE model, it was decided that no further time could be spent on debugging the model, and the subject is left for further work.

First of all, I would like to thank my supervisor Professor Jørgen Amdahl and co-supervisor Ph.D. candidate Martin Storheim for their help. Especially Martin Storheim has been to great help during the modelling work by always being available for questions and giving suggestions for solutions. Also, thanks to Erik Pettersen at Moss Maritime for making this cooperation possible. Sr. Project Engineer Karl-Anton Jacobsen at Moss Maritime has contributed with helpful considerations both regarding the technical drawings and general input on structural design aspects, and his knowledge is very much appreciated. Thanks are also given to Petter A. Hansen for being extraordinarily patient and supportive throughout countless working hours this semester. My fellow students at office C1.058 deserve mentions for providing motivation and entertainment during the last year. Lastly, I would like to thank my family and friends for their support.

Trondheim, June 10th, 2014

Heidi Jacobsen

Summary

Arctic areas contain large oil and gas fields demanding robust drilling and field development solutions. Semi submersible drilling and completion rigs are highly used for the current operations. Operating while surrounded by ice is associated with large possible damages from ice impacts. In addition, the Arctic areas are characterized by long distances and harsh climate. As commercial drilling operations are planned in among others the Beaufort, Barents and Kara sea, these complex environments need evaluation of both financial and safety risks.

The exact area of interest is to a low extent described in previous work, but many similarities can be drawn to ship collision with iceberg. The structural design is mainly based on requirements from DNV ship rules, and the relevant aspects in a collision are similar for both structures. The current ice load is conservatively assumed applied as pressure load.

Plastic considerations of plate fields before and after stiffener collapse reveal a significant demand for higher resistance towards extreme loads. Assuming large damages, the corresponding repair and strengthening costs for the considered case are estimated. Repair actions may span over a long time period due to failure of components. Hence, drilling downtime may add a significant financial risk.

Redesigning an existing structure to withstand ice loads involve numerous considerations. The pontoon skin stiffeners are seen as most prone to failure. A possible reinforcement to increase the failure capacity is stated to illustrate its effect on the impacted plate field.

Sammendrag

Arktiske områder inneholder store olje- og gassfelt som krever utvikling av robuste bore- og feltløsninger. Halvt nedsenkbare, flytende oljeplattformer er svært utbredt for disse operasjonene. Det å bore mens plattformen er omringet av is er forbundet med potensielt store skader fra islaster. I tillegg er de arktiske områdene velkjent for store avstander og harde klimaforhold. Ettersom kommersiell boredrift er planlagt i blant annet Beauforthavet, Barentshavet og Karasjøen, trengs det både evaluering av finansielle og sikkerhetsmessige risikoer i disse komplekse områdene.

Det er begrenset av utgitt litteratur innen den aktuelle analysen, men den har mange likhetstrekk med skipskollisjon mot isfjell; plattform-konstruksjonen er hovedsakelig basert på designreglementet for skip, og de aktuelle aspektene ved kollisjonen er de samme for begge strukturer. Den aktuelle islasten er konservativt påført som trykklast.

Plastiske betraktninger av platefelt før og etter kollaps av stiver avslører store behov for forsterkninger. Ved å anta store skader, kan den tilhørende forsterkningskostnaden estimeres. Reparasjonsarbeid kan vare lenge avhengig av skadeomfanget. Tapte inntekter på grunn av inaktiv tid medfører derfor en betydelig finansiell risiko.

Isforsterkning av en eksisterende konstruksjon vil involvere et bredt spekter av hensyn å ta. I det aktuelle tilfellet er pontongskallet sett som mest utsatt for skader. Ett mulig tiltak for å øke stivernes skjærkapasitet er vurdert for å illustrere virkningen på det utsatte platefeltet.

Contents

List of Figures

List of Tables

Nomenclature

Abbreviations

BC	Boundary condition
CL	Centre line
DNV	Det Norske Veritas
FE(A)	Finite element (analysis)
ICE-T	DNV-OS-C103 ice class notation for structures in transit condition
LIWL	Lower Ice Water Line
MAT	Material
SPC	Single Point Constraint
UIWL	Upper Ice Water Line
(m)USD	(Million) US dollar
WL	Water line

Greek symbols

β	$[-]$	Constant in calculation of characteristic element length
ϵ	$[-]$	Strain
ϵ_e	$[-]$	Necking strain for shell
ϵ_g	$[-]$	Uniform strain for shell
ϵ_f	$[-]$	Failure strain for shell
ν	$[-]$	Poisson ratio
ρ	$[kg/m^3]$	Material density
σ	$[MPa]$	Stress
σ_y	$[MPa]$	Yield stress
σ_{UTS}	$[MPa]$	Ultimate tensile strength
Δt	$[s]$	Time step
Δt_c	$[s]$	Critical time step
∇	$[m^3]$	Displacement

A_{col}	$[m^2]$	Area of forward corner column
A_g	[-]	Maximum uniform strain
$\boldsymbol{a_n}$		Nodal acceleration vector
A_s	$[m^2]$	Element area
B_a	$[m]$	Breadth of impact area
B_p	$[m]$	Breadth of pontoon
C	$[MPa]$	Calibrated stress constant
c	[m/s]	Material speed of sound
c_a	[-]	Constant in calculation of design ice load
c_d	[-]	Constant in calculation of design ice load
c_l	[-]	Constant in calculation of design ice load
c_r	[-]	Constant in cost estimation for repair case
c_0	[-]	Constant in initial cost estimation
C_0^{rep}	[-]	Constant in cost estimation of repair case
C_0^{str}	[-]	Constant in cost estimation of strengthening case
$\boldsymbol{d_n}$		Nodal displacement vector
e		Natural logarithm
E	$[MPa]$	Young's modulus, modulus of elasticity
F_l	$[s^2/m^2]$	Function in calculation of frame plate thickness
$\boldsymbol{F_n}$		Stress divergence vector
$\boldsymbol{H_n}$		Hourglass resistance
H_{md}	$[m]$	Height to main deck
H_p	$[m]$	Height of pontoon
L_a	$[m]$	Length of impact area
L_i	$[m]$	Length of element sides
L_p	$[m]$	Length of pontoon
L_s	[m]	Characteristic element length
$\boldsymbol{M}$		Diagonal mass matric
M	$[Nm]$	Moment
n	[-]	Function in calculation of stress-strain relationship
p	$[MPa]$	Pressure
p_h	[MPa]	Horizontal design ice load
p_v	[MPa]	Vertical design ice load
$\boldsymbol{P_n}$		External and body loads
R_m	$[MPa]$	Ultimate tensile strength
R_{eh}	$[MPa]$	Initial yield stress
R_x	[-]	Rotational degree of freedom - x
R_y	[-]	Rotational degree of freedom - y
R_z	[-]	Rotational degree of freedom - z

s	$[m]$	Stiffener spacing
T	$[m]$	Draught
T	$[ton]$	Tons of steel in cost estimation
t	[m]	Plate thickness
t_c	[m]	Increment for abrasion and corrosion
t_e	[m]	Elastic thickness requirement
T_x	[-]	Translational degree of freedom - x
T_y	[-]	Translational degree of freedom - y
T_z	[-]	Translational degree of freedom - z
$\boldsymbol{v_n}$		Nodal velocity vector
W	$[m^3]$	Section modulus

Chapter 1

Introduction

With large prospects of oil and gas resources above the Arctic circle, the market demand for robust drilling and field development solutions is increasing. The Arctic environment is extremely technically challenging, characterized by limited existing infrastructure, harsh climate and the possibility of ice encounters from both level ice and icebergs. Operating while surrounded by ice is a complex affair due to stringent station keeping demands and possible ice impacts near the water line.

Ice-capable drilling units are typically prone to high financial risks as the current drilling season in Arctic areas is limited to a few months. The existing winterized drilling rigs are not capable of handling heavier ice conditions, and can therefore not operate beyond the short summer season. However, commercial drilling operations are planned in regions such as West Russia and the Beaufort sea outside Canada and Alaska.

As collision damages pose severe risks to both crew and environment, ice reinforcement actions are required to operate safely. For accidental ice impacts some damage to the structure can be accepted, but the integrity of the hull structure maintaining the stability should not be damaged. This could potentially lead to oil or gas leakage and huge personnel risk and environmental damage, in which the latter represents a critical issue in the Arctic drilling debate. In the latest version of the DNV Offshore Standard for column stabilized units, separate strength requirements for transit in ice are added as an appendix.

The major focus of the thesis has been to establish a detailed local FE model of the bow area. This FE model is intended to use for three collision analyses in addition to the effect of reinforcement actions with the same ice load as during the collision. It is chosen to apply the ice load as a linear pressure, specifying only the initial and final limits.

However, when the LS-DYNA analyses were run on the FE model, extensive problems occurred. After merging duplicated and removing unreferenced nodes, the

program flow was clearly interrupted and LS-Dyna did not manage not initiate the analysis. This is probably due to discontinuities and geometrical changes that have occurred while remeshing or editing surfaces in the model. Debugging of such a model is very time consuming, and due to time limitations it is decided to leave the damaged model. Instead, it is focused on the simplified plastic considerations for the impacted area.

Chapter 2

Background

For previously reviewed literature, reference is made to the Project thesis [6].

2.1 MOSS CS60 drilling and completion platform

The harsh environment semi-submersible CS60 platform of the Moss Maritime type is one of about 20 floating platforms with Moss Maritime design. The typical layout consists of two longitudinal pontoons, six columns and topside with full equipment handling. Typically, the natural period lies at about 20 s. During design optimization, the resonance behaviour is attempted minimized at this frequency to control hydrodynamic loads.

As the drilling rig is intended for use in the North Sea with a harsh climate, good stability and seakeeping characteristics are essential. These capabilities are severely challenged when surrounded by ice.

The main dimensions of the CS60 pontoon and column are given in table 2.1.

Dimensions	
Length of pontoons, L_p	122.6 m
Breadth of pontoons, B_p	17.2 m
Height of pontoons, H_p	11.4 m
Height to main deck, H_{md}	38.15 m
Forward corner columns, A_{col}	12.8 x 17.2 m
Draught in transit condition, T	11.1 m
Displacement, ∇	46 000 t

Table 2.1: Dimensions of modelled drilling rig

2.2 Previous work

For the exact case of floating drilling rigs colliding with ice floes, few studies have been found. The design regulations of column-stabilized units are largely based on ship rules. Basically, analysis of a rig collision can be seen as a ship collision, since they are nearly identical in both structural layout and physical appearance.

Therefore, the present thesis work can realistically be compared to ship-iceberg collision studies. Many studies on ship collisions have been carried out and the work done by Liu, [9], is especially considered in the following.

The strength of ship structures can be varied by adjusting the parameters of the steel material model, thereby varying the relative strength of ice and ship. Typically, the collision action is characterized by kinetic energy governed by the mass of the steel structure, including hydrodynamic added mass and the speed of the two structures. Since the kinetic energy is dependent on the impact conditions, these may affect the transformation of energy after the impact. As a ship-ice collision proceeds, some kinetic energy has to be dissipated as strain energy in the steel structure, and possibly in the ice structure. This is associated with large plastic strains and may lead to significant structural damage. The energy dissipation between the two colliding objects are typically as described in figure 2.1. However, a significant part of the impact energy will remain as kinetic energy. This determination is done by assessing external and internal mechanics separately. The result of the external mechanics is the demand for energy dissipation. This result provides a useful perspective in the amount of deformations that is to be expected in the structure and the ice.

Based on Stronge [14], Liu has developed an external mechanics model with six degrees of freedom. This model is applicable both for 2D and 3D cases.

Also, a new material model was developed. Tsai-Wu yield surface was chosen to describe the iceberg ice in various loading conditions. During collision, parts of the ice structure is assumed to deform and crush. A common way to simulate failure is to use an erosion technique in which elements violating the failure criteria are deleted. Prior experience has shown that erosion does not simulate elastic or brittle failures very well due to the stress-wave issues [9]. Therefore, the ice was assumed to be perfectly elastic and plastic. The validation of the new ice model was performed by numerical examples.

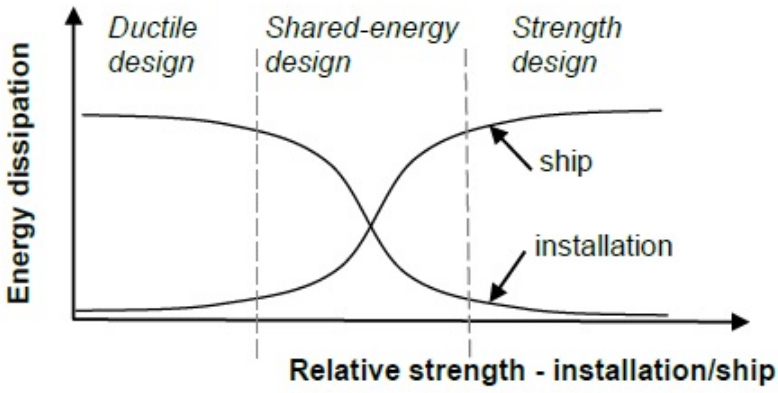

Figure 2.1: Relative strength

Chapter 3

Design requirements in transit condition

In the following a brief review of DNV-OS-C103 Appendix C, hereafter called Transit Rules, will be given as an understanding of the strength requirements in transit condition for column-stabilized units. The requirements presented are mostly those that deviate from The Rules for Classification of Ships - section *Ice Strengthening for the Northern Baltic*, hereafter called Ship Rules, which lie as a basis. In addition, the ice belt design pressure and plate thickness from the Ship Rules are mentioned.

The Transit Rules describes strength criteria for column-stabilized units intended to be navigated in light to difficult ice condition with assistance from icebreakers, when necessary.

Three notations are introduced, ICE-T(1A), ICE-T(1B) and ICE-T(1C). They correspond to the DNV ship rule notations for ice, ICE-1A, ICE-1B and ICE-1C, respectively. The Ship Rules shall, as far as practicable, determine the ice strengthening requirements for transit. In case of divergent requirements between the ICE and ICE-T standard, the ICE-T rules apply.

The CS60 unit as is is not intended to operate in ice-infested areas. As the industry intends to move drilling activity further north, the season is expanded and the possibility of meeting ice is higher. Consequently, drilling rigs could experience varying ice conditions when moving, i.e., in transit condition, either early or late in the drilling season. The rig should be able to safely pass through if encountering ice, and if so, significant structural changes are needed. For the present purpose, it is chosen to evaluate the loads equivalent to the DNV ICE-1A ice class for ships. Therefore, the **ICE-T(1A)** ice design load will be evaluated.

For more details on the requirements, see [3].

3.1 Ice design loads

Horizontal load

The design ice pressure for the ice belt region of pontoons and columns facing ice, [4], is determined by equation 3.1, which gives p $\approx 4210\ kN/m^2$. This ice pressure is theoretically associated with a level ice thickness not exceeding 0.8 m.

$$p_h = 5600 c_d c_l c_a, \tag{3.1}$$

Vertical load

The ice design pressure acting on the pontoon deck of the bow may be taken as described in equation 3.2.

$$p_v = 1200 kN/m^2 \tag{3.2}$$

3.2 Shell plating

According to the Transit Rules, the suggested structural reinforcements in the ice belt region is shown in figure 3.1.

The vertical extension of the ice belt for ice class ICE-T(1A) is stated in Table 3.1. UIWL and LIWL indicate upper and lower ice waterline, respectively. Referring to figure 3.1, the upper limit "Above UIWL" is seen as the extension above the pontoon deck.

Region	Above UIWL [m]	Below LIWL [m]
Bow	1.0	0.9
Midbody/Stern	1.0	0.75

Table 3.1: Vertical extension of ice belt

The plate thickness for longitudinal framing in ice belt regions facing ice is determined by [4],

$$t = 21.1 s \sqrt{\frac{p}{f_2 \sigma_y}} + t_c, \tag{3.3}$$

where

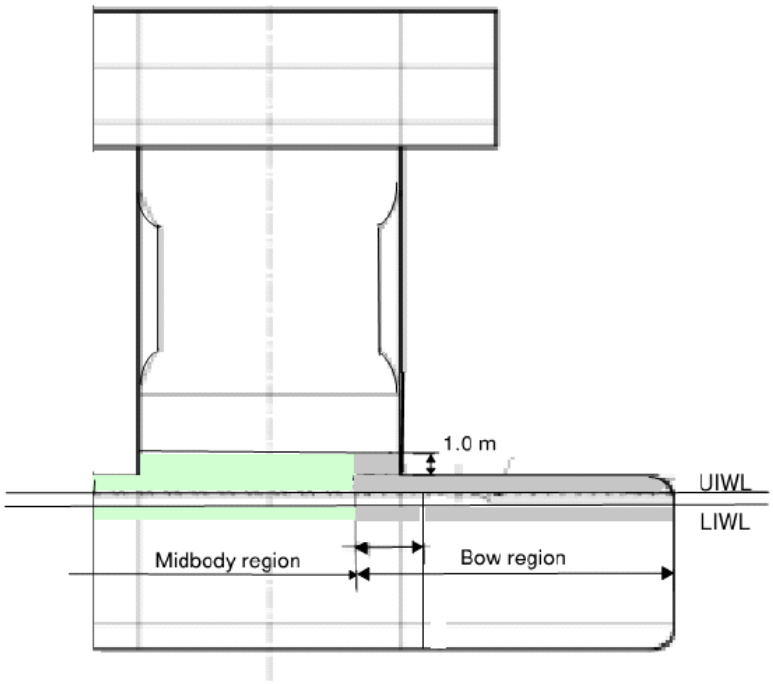

Figure 3.1: Extent of ice strengthening, [3]

$$f_2 = 0.6 + \frac{0.4}{(h/s)} \tag{3.4}$$

p is the design ice pressure as given in equation 3.1, f_2 is a function of ice reinforcement height h and stiffener spacing s, σ_y is the material yield stress and t_c is the increment for abrasion and corrosion, normally taken as 2 mm.

The basis of the plating requirement in equation 3.3 lies in elastic considerations of a plate strip. The applied bending moment is taken from the moment at mid plate, even though the maximum moment occurs at the support, i.e., the stiffeners. The mid plate moment is probably chosen due to the ability of developing membrane forces and hence increase the resistance compared to the pure bending mechanism.

The evulated stress is located at the mid span of the plate strip and is given as,

$$\sigma = \frac{M}{W} = \frac{\frac{1}{12}ps^2}{\frac{1}{6}t^2} = \frac{1}{2}p(s/t)^2, \tag{3.5}$$

and the corresponding elastic thickness requirement yields

$$t_e = \sqrt{\frac{ps^2 \cdot 10^3}{2\sigma}} = \sqrt{500} \cdot s\sqrt{p/\sigma} = 22.36 \cdot s\sqrt{p/\sigma} \tag{3.6}$$

It is observed that equation 3.3 and 3.6 are virtually equal. This verifies the elastic plate strip approach described above.

3.3 Frames

In the current model, transverse frames are found in the column front and side shell. The Ship rules requirements for section modulus and effective shear area are calculated from equation 3.7 and 3.8.

$$Z_T = \frac{pshl}{m_t \sigma_F} 10^3 [cm^3] \tag{3.7}$$

$$A_T = \frac{8.7 f_3 phs}{\sigma_F} [cm^2] \tag{3.8}$$

All of the pontoon skin and bulkheads are longitudinally stiffened. Section modulus and shear area requirements for longitudinally stiffened frames are seen in equation 3.9 and 3.10.

$$Z_L = \frac{f_4 phl^2}{m_1 \sigma_F} 10^3 [cm^3] \tag{3.9}$$

$$A_L = \frac{8.7 f_4 f_5 phl}{\sigma_F} [cm^2] \tag{3.10}$$

Chapter 4

Impact scenarios

In preparing the finite element analysis it is important to simulate realistic situations. In the following, different collision impacts will be evaluated considering the structural strength of the impacted parts.

During transit the rig is either moving on its own machine or being towed. At the transit draught of 11 m the water line lies at about the same level as the pontoon deck. Table 4.1 shows the probabilities of ice impact at each section of the rig.

For simplicity, the impact area is assumed constant. However, the pressure load is adjusted to the impacted area. The curve describing applied pressure versus loaded area is shown in figure 4.1.

As seen in figure 4.1, the pressure increases for decreasing area. The areas are between 1 and 2 m^2 large for the considered plate panels.

Ice notation	Bow	Midbody out-/inboard	Stern
ICE-T(1A)	1.0	0.85 / 0.75	0.65

Table 4.1: Probability of ice impact at each section, [3]

4.1 Bow impact

The bow area is highly exposed to being hit by ice floes, and the pontoon structure would be the most affected. Having ice floating on or above the pontoon deck also makes the lower part of the columns vulnerable to damage. This area of the CS60 rig is not reinforced for handling ice loads. The highest relative speed occurs at a head-on collision towards the bow, and this implies that the highest amount of

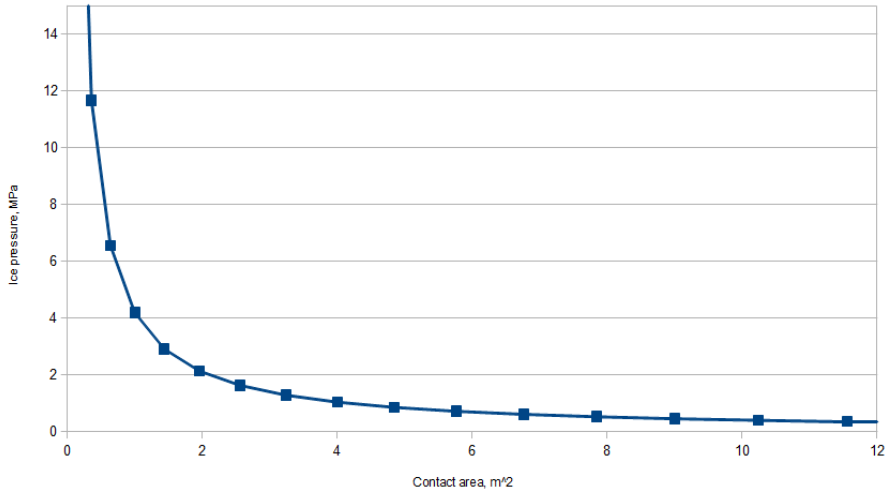

Figure 4.1: Applied ice pressure versus loaded area

kinetic energy will be available during this collision. A bow impact is thus the most critical regarding structural deformations and other damages.

Two load scenarios should be considered. A horizontal load impact on the front pontoon section and lower part of the front column will occur as the ice floes lie close to the WL. Also, a vertical impact on the pontoon deck occurs from the ice mass, in addition to the ice deflection (ice ride-down) force during a collision.

4.2 Midbody impact

The realistic midbody impacts are described below.

- Normal impact outboard side: An ice floe with forward speed normal to the outboard pontoon side may be a critical scenario. This gives a significant impact towards the longitudinal stiffeners in the skin. However, the rig forward speed will most likely limit the impact due to the varying relative angle between the ice and the rig. Since the impacted area is equal to a bow impact, this collision scenario is evaluated in the same way as for bow impact, with a somewhat smaller load.

  The ice pressure is conservatively assumed to act perpendicular to the shell plating, regardless of the actual side angle.

- Sliding impact outboard side: After a possible bow impact, the remaining

ice may side along the outboard pontoon side. The main force is directed parallel to the pontoon structure and the impact is assumed to be less fatal than a force normal to the pontoon side.

- Sliding impact inboard side: Any ice occurring between the pontoons slides along the inboard sides. Since larger ice floes most likely collide with the bow, only smaller ice bits are assumed to slide inboard. This will not lead to the harshest impact and is therefore not assessed in the present analysis.

4.3 Stern impact

As the rig has forward speed in the chosen environment, only smaller impacts will possibly hit the stern after sliding along the midbody section. Hence, a stern collision is of lower relevance in the present study.

4.4 Simulated collision scenarios

As discussed, the most critical collision scenario is the bow impact, where the relative speed is highest. According to the Transit Rules, the transition between pontoon and column shall be reinforced when the possibility of ice interaction is high. Two main collision scenarios are chosen.

Head on at bow

First, only the pontoon skin is evaluated. It is assumed that the major impact is situated below the pontoon deck, and the pressure load is applied horizontally, with one degree of freedom. The impacted elements in the bow section (black) are shown in figure 4.2. The loaded area is set to 10 m width and 1.28 m depth.

Head on at pontoon-column intersection

A more complex collision will involve the skin bow, skin deck and pontoon front side. Here, the propagation of the force distribution principle, see section 4.5, is severely challenged by the extreme pressure load, and the weaker structural elements are in great risk of failing before having transferred the load to stronger elements.

The load will approximately span over a 10 m x 2 m area, covering the most vulnerable part of the bow. The nodes to be struck by the ice load are shown in figure 4.3.

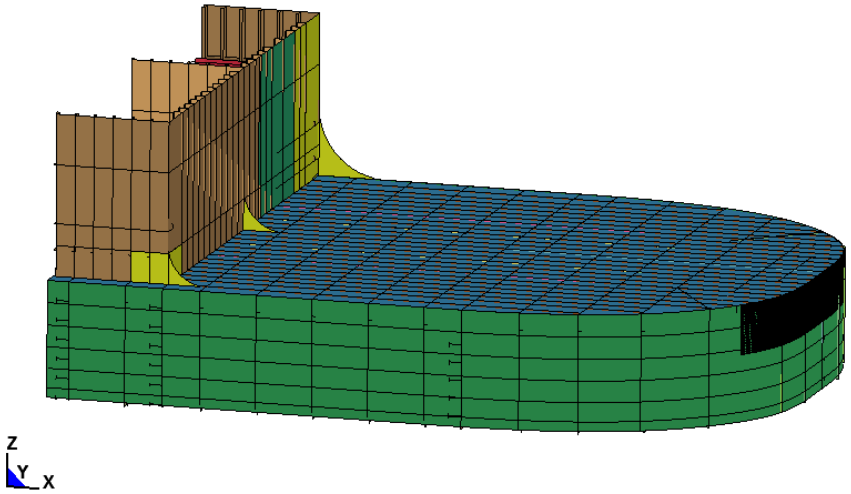

Figure 4.2: Load area at pontoon bow (black)

4.5 Expected force distribution

The following sections describes the force distribution from pressure and deck load forces and the expected force distribution during an ice floe collision.

As known from basic structural analysis the hull strength elements are organized hierarchically. The element relations from simplest to more complex are shown in Equation 4.1,

$$Plate \rightarrow Stiffener \rightarrow Stringer \rightarrow Panel \rightarrow Hullbeam, \tag{4.1}$$

where the hull beam is the internal structure, see figure 4.4.

The hydrodynamic water pressure is always at its maximum at the hull bottom shell. Also, loads from the main deck are transferred down the columns. These two loads are captured in the plates which transfer the forces to the longitudinal shell stiffeners. From here shear forces are transferred to the web frames and girders and on to the hull beam and internal longitudinal bulkhead.

The magnitude of the ice collision force could prevent the elements from transferring forces to more compound elements. The hull skin is quickly exposed to extremely high pressure and the structural response will develop well into the plastic range. Both critical buckling and shear failure may occur. When failure occurs, the impact

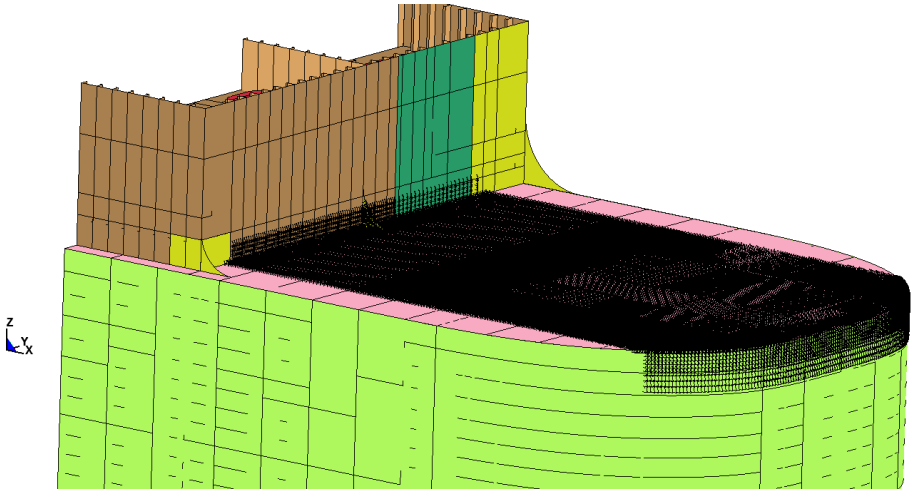

Figure 4.3: Pontoon and column load area (black)

area increases and the plating of web frames may not be sufficient to carry the loads.

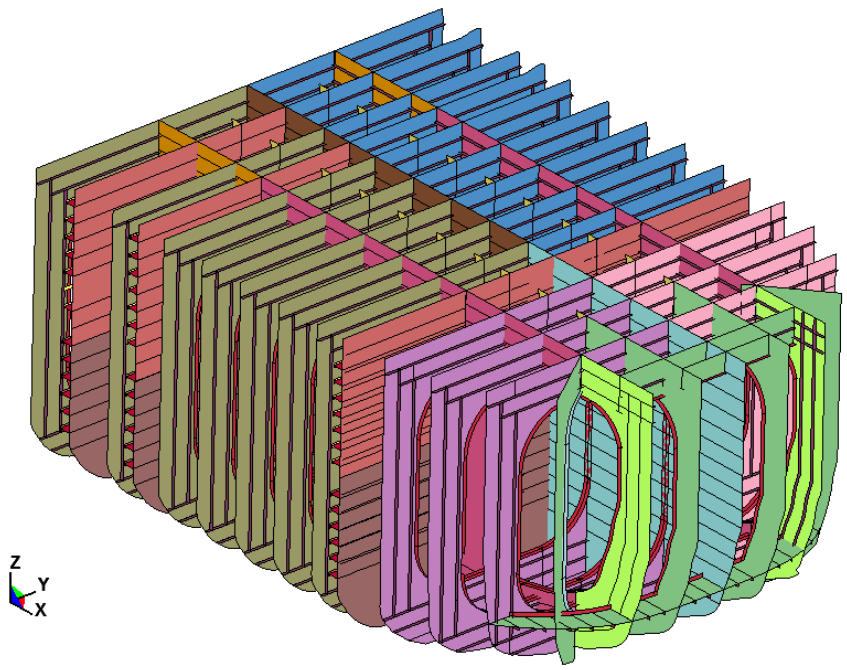

Figure 4.4: Internal structural layout, hull beam

Chapter 5

Modelling and analysis software

Three computer programs are used in the modelling and analysis part of this thesis. MSc. Patran is used for geometry modelling, LS-PrePost is used for pre- and post-processing and LS-DYNA is used for the analyses.

5.1 MSc. Patran

The geometry modelling and meshing are done in the Sesam software module Patran 2010.2.3. Patran is a powerful finite element analysis software, and provides a wide range of tools for modelling and meshing advanced geometry. Also, it may be used to compute mass and centre of gravity. Based on the finite element model, several output formats from the analysis can be written. In this thesis, input files for LS-DYNA are created.

5.2 LS-DYNA

LS-DYNA is an advanced simulation software package, with core-competency in highly nonlinear transient dynamic FEA using explicit time integration.

5.2.1 Time integration

Using the explicit central difference technique [5], the equation of motion is written as

$$\boldsymbol{M}\boldsymbol{a}_n = \boldsymbol{P}_n - \boldsymbol{F}_n + \boldsymbol{H}_n, \tag{5.1}$$

where $\boldsymbol{M}$ is the diagonal mass matrix, $\boldsymbol{P}_n$ holds external and body loads, $\boldsymbol{F}_n$ is the stress divergence vector and $\boldsymbol{H}_n$ is the hourglass resistance. Applying mid-step time integration to this equation gives

$$\boldsymbol{a}_n = \boldsymbol{M}^{-1}(\boldsymbol{P}_n - \boldsymbol{F}_n + \boldsymbol{H}_n) \tag{5.2}$$

$$\boldsymbol{v}_{n+\frac{1}{2}} = \boldsymbol{v}_{n-\frac{1}{2}} + \Delta t \boldsymbol{a}_n \tag{5.3}$$

$$\boldsymbol{d}_{n+1} = \boldsymbol{d}_n + \Delta t \boldsymbol{v}_{n+\frac{1}{2}} \tag{5.4}$$

$\boldsymbol{d}$ is the global nodal displacement vector and $\boldsymbol{v}$ is the nodal velocity vector. For each iteration, the geometry is updated by adding the displacement increment to the initial geometry. This requires many steps, but is done at a low cost per time step.

The time integration loop, [5], is seen in figure 5.1.

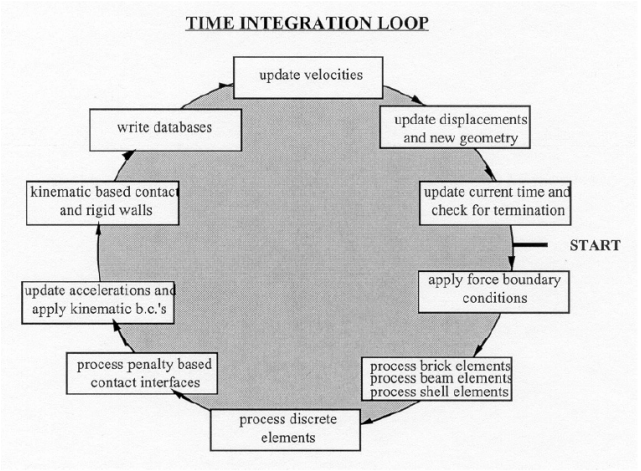

Figure 5.1: Time integration loop in LS-DYNA

5.2.2 Incremental time step

To ensure stability in the explicit dynamic finite element analysis, the time step size must be lower than the critical time step size for the model. The time step need to be smaller than the time a pressure wave uses to pass through an element. If this

is not ensured, uncontrolled pressure waves can pass through the model and cause large errors in the result, and therefore making the solution unstable. [13]

For *shell elements* the critical time step is given by equation 5.5 found in [5].

$$\Delta t_c = \frac{L_s}{c}, \tag{5.5}$$

where L_s is the characteristic element length and c is the speed sound in the material,

$$c = \sqrt{\frac{E}{\rho(1-\nu^2)}} \tag{5.6}$$

The characteristic element length can be defined in three ways:

- Length L_s calculated based on length of element size, which is the default option.
- Length based on diagonals of element. This leads to a larger characteristic length and smaller time steps, and is thus conservative.
- Non-conservative option where length is chosen to obtain large time steps. This is frequently used when small triangular shell elements are needed.

For the default option the time step can be obtained by using the characteristic length given by equation 5.7.

$$L_s = \frac{(1-\beta)A_s}{max(L_1, L_2, L_3, (1-\beta)L_4)} \tag{5.7}$$

To reduce computational costs without significantly decreasing the stability or accurancy of the model, LS-DYNA uses a process called *subcycling* or *mixed time integration*. The elements are sorted into different groups where the time step is an even multiple of the critical step size. In this way, the smallest time step during the analysis only needs to be applied to the smallest elements. The elements in this group are assumed to behave linearly between the smaller time steps.

Chapter 6

FE modelling and meshing

The following section describes the aspects considered when creating the model, especially approximate geometry, mesh type and size and chosen boundary conditions.

The semi-submersible drilling rig used in the current assessment is a Moss Maritime CS60 design, with three columns on each pontoon.

The operational draught is 23.5 m at which the displacement is approximately 70000 ton and the waterline about halfway up the columns. The transit draught is 11.1 m with a displacement of approximately 48000 ton and the waterline about up to the pontoon deck. Considering the Transit Rules, the area of interest is currently the transit draught. The steel grade is NV-36.

A model of the pontoon hull and column is used as basis for the modelling in this thesis. Only the front end of the pontoon and lower part of the column is modelled since this is the most critical section for the chosen collision scenario. Some details were excluded from the detailed model of the pontoon structure. Small brackets, manholes and detailed geometry of corners etc. are excluded since these details have limited impact on the structural strength. The surrounding structure is included in the boundary conditions which take larger support structures and dead loads into account.

To the best extent, the model is created to represent a realistic floating rig. Scantlings and drawings of the harsh environment semi-submersible drilling rig CS60 is provided by Moss Maritime AS, and all details are modelled in terms of these drawings.

The front pontoon section is modelled in detail in purpose of getting a result which represents the physics of an ice floe collision in a satisfying extent. In order to obtain realistic results, a sufficiently fine model which captures the governing deformation mechanics is important.

The CS60 is symmetric about the transverse axis. As the original drawings only show the aft end in detail, these are used to model the desired front end. For the present purpose the pontoon is modelled from frame -1 to 12 and the front column from frame 9 to 12.

6.1 Geometry

Small penetrations are discounted in this particular model, as they will not affect the global load paths through the structure.

6.1.1 Pontoon skin

The bow curvature is drawn from model test coordinates. Looking aft, the two-dimensional curvature changes into a rectangle with curved lower corners. Stiffeners on the hull skin are made by dividing the shell in smaller surfaces and extruding the intersection curves between the surfaces to form the stiffener web height. The web height is 250 mm. The stiffeners are modelled as L-stiffeners with flange length 90 mm. The pontoon shell is longitudinally stiffened with spacing of approximately 650 mm and web frames with spacing 1900 mm.

6.1.2 Pontoon internal structure

Due to identical web frames, only one issue of each unique frame is modelled and then translated to the current position. Some details are left out.

The pontoon is stiffened with three longitudinal frames, see figure 6.1. The bulkhead at CL has longitudinal L-stiffeners, while the stringers spaced 3840 mm apart from CL have flat bar stiffeners around the tank room holes. Also, there are one stringer spaced 1920 mm on each side of CL to support heavy deck load.

With some exceptions, transverse web frames are spaced about 1900 mm apart along the longitudinal direction. Most of these are cut-out tank room frames with flat bar stiffeners, while three frames are bulkhead and half bulkhead-half web frames with L-stiffeners. Frames are modelled drawn curves and hereafter from the corresponding extruded surfaces.

In addition, the web frames are supported by the mezzanine deck with L-stiffeners.

6.1.3 Column

Close to the pontoon deck the column cross-section is rectangular with sharp edges, approximately L_a x B_a = 17 m x 13 m. The total height of the columns is 25 m. As mentioned, only the lower part is modelled.

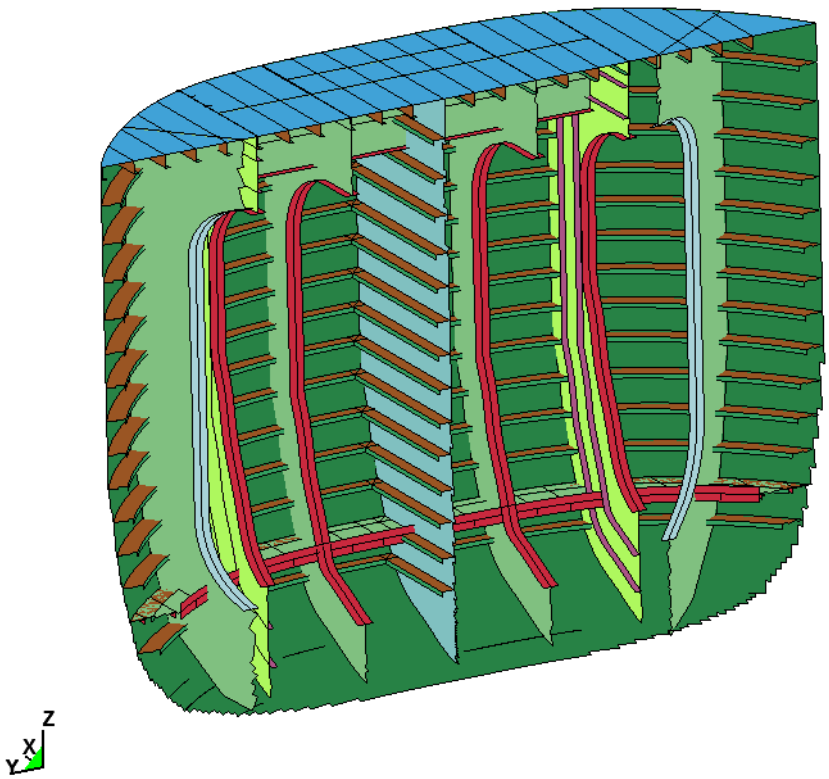

Figure 6.1: Bow longitudinal geometry

6.2 Meshing

To obtain accurate results for large indentations, the model is meshed with fine mesh in all of the bow area. Since the mesh forms the basis for describing the geometry and mechanisms involved in the physical model, the results obtained from the mesh will strongly depend on the mesh used.

4-node Belytschko-Tsay shell elements with five integration points over the thickness are used as the main element type for the entire model. In regions with advanced geometry 3-node shell elements are used to avoid very small critical time step. According to [10], the use of 3-node elements should be limited due to less accuracy compared to 4-node elements. 3-node elements are therefore only used where the gemeotry requires and where the 4-node elements turnes out to be too

large.

The mesh size is important to consider. Elements with large aspect ratios will have a significant impact on the total computation time, that is, severely increase it. Alsos, [1], carried out a convergence study of a ship grounding scenario, and this study can be adopted into the present collision scenario. This study concludes that, in order to give a good physical approach, the element length should be 5 to 10 times larger than the plate thickness. The CS60 shell thickness varies between 15 and 40 mm, while the stiffener web thickness varies from about 10 to 20 mm. The mesh sizes are then in the range 80-300 mm for the shell and 60-150 mm for the stiffeners.

Choosing appropriate mesh sizes is essential to get a satisfying result. Fine mesh is required to capture strain concentrations and fracture and is thus necessary. The finer the mesh, the more elements and longer computation time is needed. A coarse mesh will not capture strain concentrations typically seen in ship structures. As the pontoon structure is designed very similar to a ship structure, the same conclusion holds for the present drilling rig; strains rising during the collision will not be accurately measured. Also, since the CS60 is not ice-strengthened, it is of even higher interest in this thesis to capture the collision aftermath. In order to reinforce the structure, the strain data captured will reveal one of many aspects of the structural behavior. In addition, the strain data shows how the steel material experiences the collision.

Ideally, 4-node elements should be perfectly shaped quad-elements with aspect ratio equal to one. In regular shaped areas this is achieved, but in areas with advanced geometry, e.g. curved surfaces, the elements will be distorted. It is desirable to minimize the use of distorted elements to obtain accurate results. The troubled areas are divided into smaller surfaces that are more easily meshed as quadratic elements, while curved or advanced surfaces are meshed using Paver mesh type.

The element size results in a large amount of elements, approximately 500 000 for the model. In consultation with PhD candidate Martin Storheim this is found to be an acceptable number of elements for the purpose used. All of the front model will be largely impacted during a collision, and reducing the number of elements in parts of less relevance will therefore not be beneficial for the results. As more elements give a more accurate result and small elements severely increase computation time, the current number of elements should be an acceptable compromise between element sizes and accuracy.

Surface coupling is required to realistically transfer stresses and forces. Mainly, the final mesh from MSc. Patran is the basis for the structural connections. Most of the free edges have been eliminated by remeshing or completely redrawing the surfaces, while some are still present in some areas. Ideally, these free edges should be completely fixed, but it is considered that a sufficient force distribution happens with some loose ends present.

6.3 Properties

The pontoon model is divided into several different groups. The groups are based on thickness properties from the structural drawings of the drilling rig. This made the modelling easier as one can view a selection of groups when creating new geometry, in addition to making the post-processing better organized. Selected parts of the model can then be viewed based on their property to assess local components.

6.4 Analysis settings

Many studies on floating structure collisions have been carried out and many simplifications are used to decrease the computation time. With the selected options, sufficient computation time is obtained. This is only an approximation to simulate a real collision scenario, and it is interesting to compare the results from such an analysis with a more realistic situation.

When simulating a more realistic collision between a floating drilling rig, one or both of the colliding bodies are given an initial velocity towards the other body. Consequently, they will behave as if they were in a real collision, as the energy dissipates between the two bodies throughout the time span of the simulated collision. A head-on collision leads to the harshest impact on the structure, since the relative speed and force components are at their maximums in this position.

6.4.1 Material

High tensile strength steel is used for all modelled parts. This corresponds to the steel grade NV-36 used in the original drilling rig, only with plastic properties to explore the ultimate capacity. The chosen material provides elasto-plastic behaviour with isotropic power law hardening. It is used by Liu [9], and found sufficient to use for the assessed structure.

The material properties are calibrated using the procedure outlined in Zhang, [8]. Both geometrical and material nonlinear structural effects are involved, and the input of material properties up to the ultimate tensile stress has as significant influence on the extent of critical deformation energy. It is generally recommended to use true stress-strain relationship as obtained from a tensile test,

$$\sigma_y = C\epsilon^n = C(\epsilon_{yp} + \bar{\epsilon}^p)^n, \tag{6.1}$$

where

$$n = ln(1 + A_g), \tag{6.2}$$

$$C = R_m(\frac{e}{n})^n \tag{6.3}$$

ϵ_{yp} is the elastic strain at yield, while $\bar{\epsilon}^p$ is the effective plastic strain.

A_g is the maximal uniform strain related to the ultimate tensile stress R_m and e is the natural logarithmic constant. For shipbuilding steel the following approximation can be used to obtain proper A_g value from a known R_m ([MPa]) value,

$$A_g = \frac{1}{0.24 + 0.01395R_m} \tag{6.4}$$

Calculations with LS-DYNA have shown that the deformation energy responds very sensitively to the defined failure criteria. The defined failure strain value is the most important key point for a correct prediction of realistic critical deformation energy, and hence, an improper failure criterion can lead to an incorrect assessment of the energy absorption. [8].

Usually the first rupture of an element in a finite element analysis will be defined with a failure strain value. Once a shell element exceeds the defined value, it is deleted from the finite element model. The deformation energy in this element will keep at a constant value in the further calculation steps. Scharrer, [12], recommends the definition of failure strain as seen in equation 6.5.

$$\epsilon_f(l_e) = \epsilon_g + \epsilon_e\frac{t}{l_e} \tag{6.5}$$

The numerical material properties are shown in table 6.1.

Parameter	Symbol	Value
Density	ρ	7850
Poisson ratio	ν	0.3
Ultimate tensile strength	R_m	490-630 MPa
Yield stress	R_{eh}	
t $<$ 25 mm		355 MPa
25 mm $<$ t $<$ 50 mm		335 MPa
Maximal uniform strain (UTS)	A_g	0.14133
Hardening exponent	n	0.13217
Strength coefficient	C	731 MPa
Uniform strain for shell	ϵ_g	0.056[−]
Necking strain for shell	ϵ_e	0.54[−]

Table 6.1: Material data

6.4.2 Boundary conditions

It is difficult to apply realistic boundary conditions for the front pontoon section when the global drilling rig model is not included. As previously described, the pressure load is applied over a number of time intervals and is considered as the colliding action. In a real situation, small ice floes will collide with the drilling rig, and the ice will slide away. In this case, the ice strength is small relative to the drilling rig. However, heavier ice conditions can lead to ice floes crushing onto the pontoon and column structure, and major deformations will form. The latter case is of most relevance in order to assess the possible damages to the drilling rig.

Several options for boundary conditions exist, and the consequences of choosing inertia controlled and pinned boundaries should be considered. In the inertia controlled conditions, the mass of the whole rig is included as a distributed mass along the boundaries. For pinned boundaries, no moment forces should push the side. According to Martin Storheim, [13], the two different options are practically identical when comparing maximum indentation. Since pinned boundaries give satisfying results, they are chosen for the current model.

The model length is chosen so that the front part of the column is included. At the aft end of the model, both the pontoon and column have larger support frames. Hence, the pinned boundaries are realistically applied at the location of these frames to correspond to the actual structure. The top end of the column is pinned to represent the rest of the structure and to allow rotation.

6.4.3 Mass and added mass

For the modelled front section, the mass and added mass will not contribute to the results due to the pinned boundary conditions.

Chapter 7

Analysis setup

The chosen analysis setup in LS PrePost is described in the following.

Load

The ice pressure corresponds to the design load described in section 3 and Appendix C in [3]. As a collision load drastically increases over a short time span, the load applied load will capture this fact. Due to time limitations, it is chosen to apply the ice collision load as pressure load.

A load curve is defined using *DEFINE_CURVE, and a series of time versus load points is plotted. The load details are shown in figure 7.1.

Material

Material 18, *MAT_POWER_LAW_PLASTICITY, is used in the current analysis. The material data is given in section 6.4.1.

Boundary conditions

Based on the information described in section 6.4.2, pinned boundary conditions are chosen for the model. Pinned boundaries are applied to all nodes both on aft sides of the pontoon and column and top sides of the column. This is the most simple boundary condition regarding both application and computation time, and the error of this method will be investigated further in the analysis of the results. The boundary conditions are shown in table 7.1.

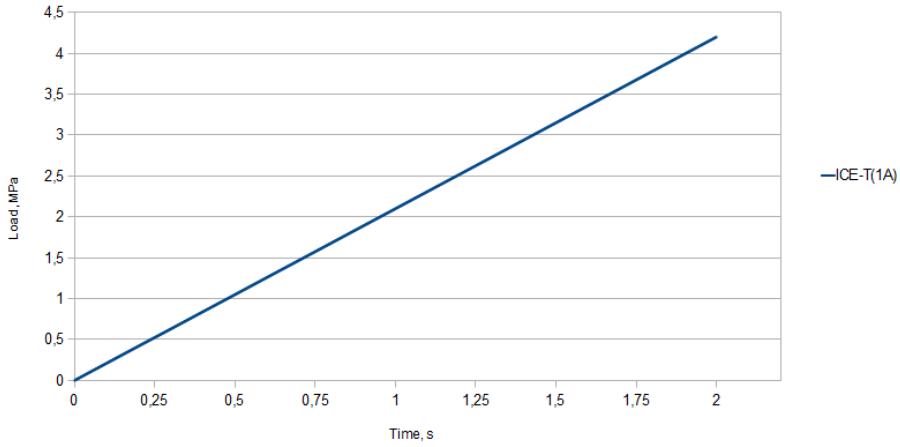

Figure 7.1: Applied load as function of time

	Translation			Rotation		
Side	T_x	T_y	T_z	R_x	R_y	R_z
Aft pontoon side	1	1	1	0	0	0
Aft column side	1	1	1	0	0	0
Top column side	1	1	1	0	0	0

Table 7.1: Boundary conditions for the analysis

Controls

*CONTROL_HOURGLASS controls the zero energy modes which arise using one-point integration. More on hourglass modes is found in the LS Dyna theory manual, [5]. The hourglass energy is included in the energy balance using the *CONTROL_ENERGY command. *CONTROL_TERMINATION defines the end time. This corresponds to the load curve end time. The collision duration is set to 2 s with time steps of 0.02 s, i.e., 100 steps in total.

Output options

The structural data to be analyzed and stored as output data is shown in table 7.2.

Option	Keyword	Time interval between outputs [s]
Global statistics	GLSTAT	0.02
Material energies	MATSUM	0.02
Resultant interface forces	RCFORC	0.02
Animation	D3PLOT	0.02
hline		

Table 7.2: Output data

Chapter 8

Results

The results from the conducted analysis are presented in three sections. Firstly, the plastic calculations are described and evaluated. The found pressure forces and corresponding deflections are compared with the resistance of the impacted structure. Next, structural reinforcements are suggested, and the "new" resistance is assessed. Lastly, the costs of ice-strengthening the current structure (seen as a new-build drilling rig) are evaluated against repairing damages that rise from the applied ice force.

As the intended results from non-linear FEA are lacking, the current assessments are limited to simplified plastic considerations. The FE model and analysis will be further commented in the section for further work, section 9.2. The damaged model is enclosed, see appendix B for details.

8.1 Damage prediction by plastic considerations

As the CS60 rig is not reinforced for ice, applying ice pressure corresponding to heavy ice condition will lead to significant deformations and failure of structural elements. There are many failure modes which must be considered in the analysis of the rig structure, and these modes can range from local failures to large scale global structure failures. The resistance analysis described in the Marintek report [2] is used to outline the procedure for the present analysis. Appendix A holds the files used for the plastic analysis.

The resistance to ice pressure is checked in a hierarchical manner. First, the capacity of the plating between stiffeners is estimated by means of plastic theory allowing large deformations. Then, the capacity of the stiffeners with associated plate flange is addressed using plastic mechanism theory. Finally, the resistance of web frames and possible collapse of them is commented.

The structure assessed is a typical (ship) hull structure, consisting of steel plating reinforced with longitudinal stiffeners and transverse web frames. Moderate plastic deformations are normally accepted. Currently, no clear definition for the amount of allowable plastic deformations exists for design of ice-strengthened structures. Minor indentations in hull plating may not be repaired immediately, but must be considered at the next scheduled overhaul. The magnitude of the indentation may also require repair sooner than anticipated. In turn, this relates to the cost issue of allowing deformations.

The current assessment is based on the actual structural resistance and the design ice load given in [3]. No safety factors are assumed, but updated structural resistance is easily found by adding them to the formulas used for assessment.

8.1.1 Capacity of plates

The steel plating experiences permanent plastic deformation from the ice pressure. The plate deformation is greatest between stiffeners and frames and can result in the hull structure exhibiting a "hungry horse" appearance. The longitudinal stiffeners exacerbate the deformation due to the large width-to-height ratio of the load area, whereas a transversely stiffened panel would pose more resistance per width.

It is most likely to have impacts along the pontoon side and at the column sides. The vertical load impact described in chapter 4.1 is briefly commented. The pontoon deck has the same properties as the skin side, and the vertical design load is significantly smaller than the horizontal. Therefore, the deck impact is less comprehensive than the side impact, and is considered of less practical relevance. The shell plate thickness is 16 mm, while the column has 15 to 40 mm plates along the front side.

The plastic capacity of shell plating is several times larges than predicted by linear elastic theory. As the deformations become finite, membrane forces develop. The plate will yield, but still the capacity increases because of the geometric effect. Figure 8.1 shows pressure versus maximum plastic deformation of the shell plating, in which both the relative displacement and load capacity are made non-dimensional. Up until the displacement-thickness ratio is 1, the plate carries the load by bending. In the linear region $w/t > 1$, all load-carrying is done by combined bending and membrane action.

It is noticed that the column shell has lower load-carrying capability than the pontoon shell. The lower part of the column has smaller length-to-width ratio and this implies stiffer plating, less allowable deflection and less membrane forces.

The critical pressure load leading to plate failure is limited by fracture. Initiation of fracture is predicted by the method given in NORSOK N-004 Annex A, [11]. See Appendix B for information about the detailed calculation. The results of the plate rupture analysis are given in table 8.1.

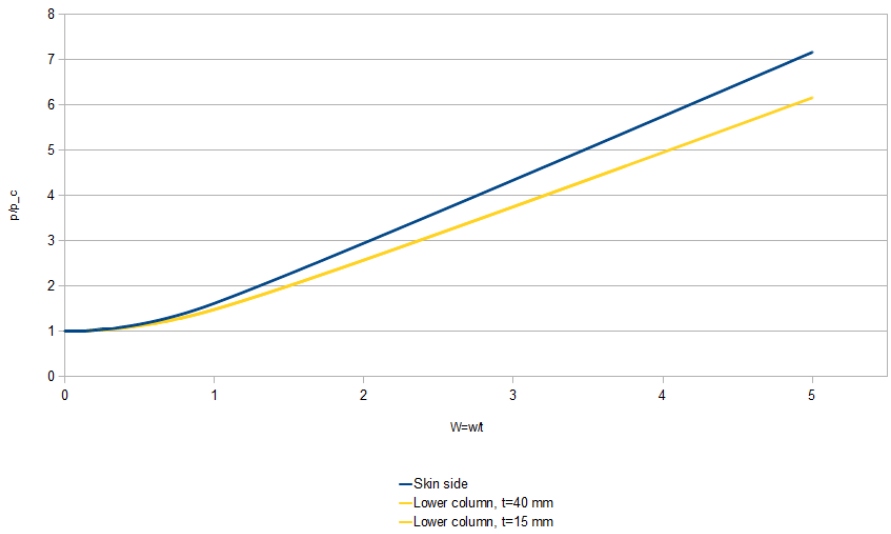

Figure 8.1: Load-carrying capacity of shell plate as function of lateral displacement

Location	Critical pressure	Rupture deformation $[w/d_c]$ / [w]	Applied uniform pressure	Corresponding deformation $[w/d_c]$ / [w]
Skin shell	7.2 MPa	3.8 / 61 mm	5.2 MPa	44
Skin deck	10.5 MPa	5.6 / 73 mm	1.2 MPa	10
Column, t=15	7.7 MPa	4.3 / 65 mm	3.2 MPa	26
Column, t=40	12.7 MPa	0.7 / 29 mm	3.2 MPa	

Table 8.1: Critical pressures and deformations for the impacted plates

For the skin shell, the critical pressure for rupture is 7.2 MPa with a corresponding deformation of 61 mm. The distributed pressure across the impacted area, 1.92 x 0,64 m, is 5.2 MPa, which produces a deflection of 44 mm. This is lower than the capacity of the plating, and the skin is considered to resist the pressure load.

As mentioned, the skin deck has much of the same properties as the skin side. With 13 mm plating, the expected critical pressure lies at 10.5 MPa, which will give 73 mm deflection. The applied load is only a fraction of the critical, and the deformation of 10 mm is well inside the tolerable limit.

At the lower part of the column, the 15 mm plating is found to deflect 65 mm before rupture, corresponding to 7.7 MPa. As the impacted area here is somewhat smaller than assumed at the bow, the ice will lead to a pressure of 3.2 MPa and an associated deflection of 26 mm. The 40 mm plate at the outboard side ruptures

at a pressure load of 12.7 MPa, and has significant excess capacity.

At all considered locations the maximum ice pressure will cause the plates to fail if the contact area is smaller. However, as small ice floe areas are characterized with between 20 and 50 m^2, rupture of these single plates are not considered likely due to major membrane forces.

8.1.2 Capacity of stiffeners

The capacity of stiffeners is calculated using plastic mechanism theory by the same procedure as used in chapter 8.1.1. It is assumed that the pressure is uniformly distributed over the stiffener between two transverse frames. When the stiffener undergoes finite deformations, membrane forces may develop, but this effect is considered to be small for stiffeners and is here neglected. Hence, a stiffener will behave significantly stiffer and fail much earlier from deflection than a plate when exposed to lateral load.

For the stiffeners in the impacted area, the critical deformation for rupture is found to be only 1.5-5 mm, see table 8.2. This calculation is very uncertain due to the distorted cross-section when the stiffener laterally deflects at midspan. Tensile stresses are then relaxed, and the rupture calculation is no longer valid.

It is noticed that the critical location for tensile fracture is at the top flange of the stiffener, while the strain in the shell plating is considerably smaller at the same time. Rupture in the shell is therefore practically only dependent on the stiffener rupture.

Location	Critical pressure	Pressure over loaded area
Skin	0.51 MPa	5.2 MPa
Column	0.77 MPa	3.2 MPa

Table 8.2: Critical pressures and deformations for stiffener failure

The critical load for the skin stiffener considering the cross-sectional strength is 0.51 MPa. The highest ice pressure of 5.2 MPa is assumed at the bow plate panel. Hence, the stiffener will not resist the pressure, but will collapse. For the column, it is also found that the applied load will make the stiffener fail.

8.1.3 Resistance after stiffener collapse

When stiffeners collapse, the deformations extend to adjacent plate fields. Also at these deformations, membrane forces develop in the plating. The lateral component of the membrane forces has to be supported by adjacent, intact stiffeners and adjacent web frames. If the stiffeners resist this load, the deformation field is final. Otherwise, the deformations extend to the next plate field. [2]

When a stiffener fails, the loads are transferred partly to the adjacent stiffeners and partly directly to the adjacent web frames via shell plating. The total load transferred to the adjacent stiffener is estimated by equation 8.1,

$$\begin{aligned} p_{st} &= (0.5 - 0.25\frac{b}{l})pA_{loaded} \quad \text{if } b < l, \\ p_{st} &= 0.25\frac{l}{b} \qquad\qquad\qquad\qquad \text{if } b > l, \end{aligned} \tag{8.1}$$

where b is width of the deformed area and l is web frame spacing, p is ice pressure and A_{loaded} is loaded area. It is assumed that the load is transferred equally to frames and stiffeners within a distance $b/2$ of web frames, otherwise solely to stiffeners. The resulting pressures and deformations are shown in table 8.3.

Location	Loaded area [m*m]	Deformed area [m*m]	Local coll. pr. [MPa]	Avg pr. [MPa]	Limit def. [mm]
Skin panel	1.92*0.64	1.92*12.2	5.2	0.27	61
Column, t=15 mm	1.19*0.64	1.19*1.92	3.2	0.65	65
Column, t=40 mm	1.19*0.64	1.19*1.92	3.2	0.65	29

Table 8.3: Deformations in side plating assuming failed stiffeners

In the column, three stiffeners are likely to fail. They exert the same behaviour for both the 15 and 40 mm plates, but the the thinner plating is more flexible and allows larger deflections. This is due to higher membrane forces, which are much more limited in the 40 mm plate. In both cases, the applied load is less than the critical plate rupture load. Hence, column plate failure is not expected. It is however advised to reinforce the lower column either by more solid brackets or plates in the pontoon-column intersection or by add a supporting structure at the pontoon bow to limit the amount of possible ice floes on deck. The latter also minimizes the vertical deck load from the ice.

19 skin stiffeners are likely to fail before the distributed load can be handled by the stiffener strength. The total load without these stiffeners amount to a deformation of 73 mm. This is beyond the critical limit for the skin plate, 61 mm, and the plate will therefore fail. Major structural damages may be assumed after these findings. The force will develop further into the nearby web frames, which are likely to fail from buckling.

8.1.4 Further development of damage

At the lower column the ice pressure effect is lower than the critical stress for plate rupture. Hence, it is concluded that the stringers will resist the load such that the deformation field is final. Three stiffeners will collapse.

It is noticed that the plastic methods used assumes that a centre stiffener collapse first. From here, the collapse load is transferred to the adjacent stiffeners. In the present case, the ice pressure would hit the stiffeners at the top of the skin side first. The load transfer is therefore only done in one direction. The skin side holds less than 19 stiffeners along the height of the pontoon, and the force distribution may prove to be different than found here. If twice the impact load where to be transferred down the pontoon side, plate rupture would occur at an earlier stage. The larger structures such as girders and web frames will then be exposed to massive loading. In this case, the forces are way beyond tolerable limits for the hull beam. The front end of the CL girder is 18 mm thick, and will not sustain these loads. Failure by buckling is likely to happen.

Ideally, the global integrity of the structure should remain intact. This relates to hydrostatic stability and hull girder strength. With the assumed ice force, major rupture of the plating will break the "sequence" of force distribution. Also, the hull girder bending moment and shear force in flooded condition should be added to the dynamic bending moment and the force. As hydrodynamic forces are not specifically considered in the present thesis, this aspect for global reaction forces is left for further work.

8.1.5 Calibrated failure strains

For tensile fracture in plates, the critical strain is taken as the strain given in [11]. For high tensile steel, a critical strain of 15% is proposed. The applied material properties as implemented from [8] allow calibration of failure strains for the different components, see figure 8.2. For details about the calculation, see Appendix B.

As the constant critical strain assumed in [11] is set somewhat higher than the calibrated failure strains, the results found are non-conservative. The expected plate ruptures therefore occur at an earlier stage. For the skin plate, the rupture deformation may be as much as 25% smaller, i.e., at 49 mm. Due to the extreme ice load, the structure is found to not resist the forces even with a critical strain at 15 %. Severe damage will cause the structure to undergo unbearable deformations, and smaller critical strains will not significantly change the reaction of the structure.

8.2 Suggested reinforcements

In the following, it is attempted to decrease the damages found from chapter 8.1 by increasing the strength of the most vulnerable sections. The CS60 as is clearly needs major structural changes to withstand the applied ice load. The reinforcements considered will still allow some plastic deformations and the corresponding repair costs in a certain time interval.

Stress-strain calibration (Zhang, 2004)

UTS (Rm) range	490	Mpa	to	630	Mpa
Ag	0,1413	-			
n	0,1322	-			
C	730,7690	Mpa			
Failure strain with respect to plate thickness					
eps_g	0,056			e_y	0,001690476
eps_e	0,54				

Plate thicknesses, mm	Approx. Element length, mm	Failure strain	UTS, Mpa
8	70	0,118	550,7
9	70	0,125	555,4
10	80	0,124	554,2
11	80	0,130	558,2
12	80	0,137	561,9
13	80	0,144	565,5
14	100	0,132	558,9
15	100	0,137	561,9
16	120	0,128	556,9
18	120	0,137	561,9
20	150	0,128	556,9
22	150	0,135	560,9
25	200	0,124	554,2
30	200	0,137	561,9
45	300	0,137	561,9

Figure 8.2: Calibrated failure strains with respect to thickness

The study conducted by Kujala and Ehlers in [7] aims to identify acceptable and probable plastic deformations based on the requirement and expenditure to repair these damages. The transversely stiffened bulk carrier MS Kemira is evaluated by strain gauges is order to assess the deformations from ice-induced loads. A plate panel is exposed to the maximum load measured to occur within 1-, 2-, 3-, 5-, 10- and 20-years. Using a plastic deformation limit of s/10 for the reference structure, the resulting repair costs are shown in figure 8.3. It can be seen that the repair costs are decreasing for increasing design load levels, while the corresponding production costs are found to increase with increasing load levels.

According to [7], increasing the design load level by 18% and hence decreasing the repair costs by 62% is suggested. This can be seen as one of many possible solutions towards optimizing reinforcement cost versus repair costs. Other factors such as global stability and movements in all degrees of freedom are excluded in the present thesis.

The suggested reinforcements are solely increasing the structural strength to an extreme ice load. Due to the CS60 design, it is however chosen to increase the stiffener capacity beyond 18%. This will largely improve the load strength, even though some stiffeners still fail from the loading. The plate capacity is aimed to be sufficient to withstand the failed stiffeners, so that the total plate field is still intact. Optimizing repair costs for the current structure requires a complex study for the entire structure, and only the basic reinforcements are presented in this thesis.

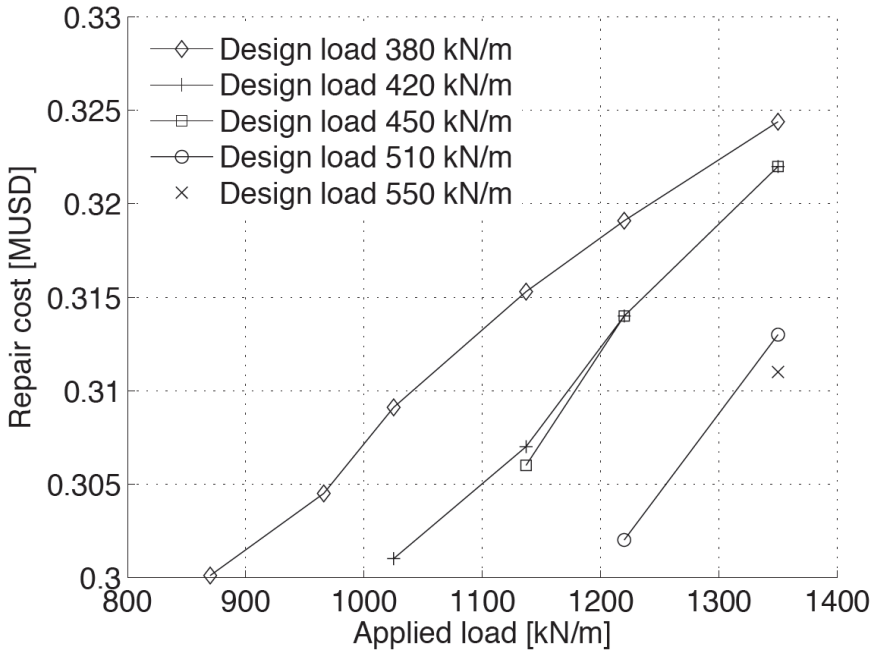

Figure 8.3: Repair cost as a function of possible higher design load, [2]

8.2.1 Skin plate and stiffeners

In order to enable the stiffeners to carry the applied load, it is chosen to decrease the frame spacing to 1000 mm. Hence, each stiffener and plate field has a loaded area of 0.64 x 1 m, which is about half the area they currently have. The web thickness is increased from 10 to 15 mm. Table 8.4 shows the planned changes and the corresponding critical load and deformation.

The ice-induced plate deformation reflects the deformation occurring from the applied ice load, 4.2 MPa. From the chosen reinforcements of the skin panel, it is likely that three stiffeners will fail. The plate is then deflecting 22 mm, which is safely within the critical deflection of 51.1 mm. As long as the deformation field becomes final, this indentation may be accepted.

8.2.2 Column plate and stiffeners

For the column, the stiffener is the critical component with respect to strength. The web thickness is here increased to 15 mm, while the frame spacing is kept the same. The corresponding increased pressure and deformation resistances are

Parameter	Value
Frame spacing	1000 mm
Plate thickness	20 mm
Stiffener web thickness	15 mm
Critical pressure, plate	13.2 MPa
Critical pressure, stiffener	1.62 MPa
Critical deformation, plate	51.1 mm
Critical deformation, stiffener	1.36 mm
Ice-induced plate deformation	22 mm

Table 8.4: Reinforced profiles and corresponding capacity for skin

Parameter	Value
Frame spacing	1190 mm
Plate thickness	15 mm
Stiffener web thickness	15 mm
Critical pressure, plate	7.7 MPa
Critical pressure, stiffener	1.4 MPa
Critical deformation, plate	65 mm
Critical deformation, stiffener	1.61 mm

Table 8.5: Reinforced profiles and corresponding capacity for column

seen in table 8.5. With these dimensions, one stiffener will fail and the transferred load is sufficient for the adjacent stiffeners to withstand. Hence, the load field is considered sufficient for the current impact.

8.3 Cost estimations

As more oil based industry moves towards ice covered areas, risk and cost analyses may be helpful as guidelines on whether drilling actions in ice are justifiable or not.

Kujala and Ehlers, [7], investigate the balance between the two extremes in ice-strengthening of hull structures. It is possible to increase the scantlings until no plastic deformations occur during the lifetime of the structure, but at a higher investment cost. Consequently, no repair costs are needed during the design life. The other possibility is to allow some local plasticity requiring repair work at specified nominal frequencies, which causes smaller investments, but higher maintenance costs. The evaluation is carried out using long-term measurements of ice loads and their probability of occurrence for the example ship MS Kemira.

Currently, there are no clear limits for the amount of allowable plastic deformation for the design of ice-strengthened ship structures. Kujala and Ehlers assume that a reasonable value that requires repair is $1/10^{th}$ of the stiffener spacing. Also,

an allowable deformation of 1/20 s is assumed to conduct a sensitivity study on the deformation versus repair cost. The corresponding ratio is seen in figure 8.4. As expected, the study shows a significant increase in repair cost as the plastic deformation limit decreases. By allowing only a repair deformation of 1/20 s, the repair cost is increased by a factor of 2.5 compared with the cost when the deformation limit is 1/10 s.

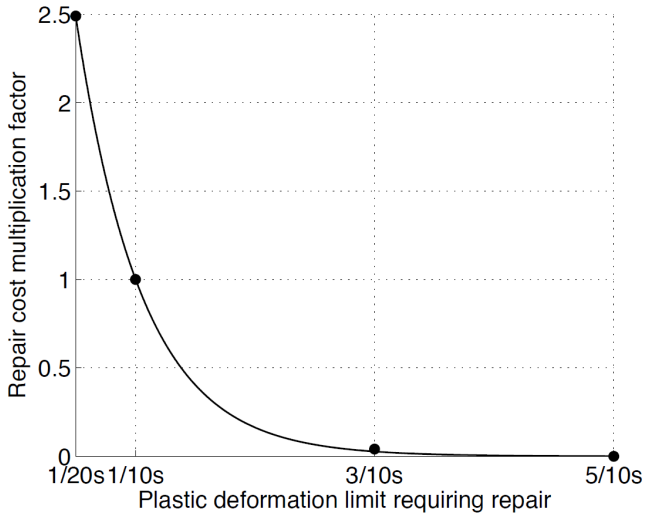

Figure 8.4: Sensitivity of the repair cost to the deformation limit requiring repair, [7]

The sections studied in detail include mass properties calculated in MSc. Patran. The suggested reinforcements are based on percentage increase of mass of the considered component. For other cost factors, approximate values are used. For more details on the cost estimation, see enclosed spreadsheet in Appendix B.

Costs of ice-strengthening

Considering additional masses due to increase of web and plate thicknesses and reduced frame spacing, the present strengthening requires about 220 extra tons of steel. Ice-strengthening the two pontoon bows hence increases the total structural weight by 1.5 %. Here, only reinforcement of skin and column is assumed.

Costs of repair actions

The extent of the repair cost is estimated by assuming a certain percentage of each component needing replacement. Skin and column plate, stiffener, web frame and bulkhead/girder masses are multiplied by a factor estimated as repair percentage of the entire part. The total mass to be replaced sums up to about 280 tons.

In lack of relevant repair costs, the suggested rates stated in [7] are used. European repair cost rate per kg is assumed, and a downtime of 10 days due to the repair

actions is chosen to give a picture of the possible off-hire costs. The rates used are assumed equal to the bulk carrier costs in the mentioned study. Finally, the repair cost is found to be about 6 mUSD.

Chapter 9

Conclusions and further work

9.1 Conclusion

Floating structures moving in Northern areas are expected to increase the following years due to increasing petroleum operations. Semi-submersible drilling rigs used in these areas will be prone to ice-induced loads of varying severity, and worst case consequences may involve leakage, capsizing and pollution.

A local bow model has been created and attempted analyzed for three different impact locations. The total number of elements in the rig structure is about 500 000. The element sizes vary from 70 to 300 mm and could be smaller to get a more accurate results. This is a topic for further work. The considered ice floe impact is applied as a pressure load corresponding to the Transit Rules design ice load. The steel material properties are calibrated from the procedure outlined by Zhang, and is not verified, but assumed to be reliable for the current analysis.

Plate panel collapse analysis for the scenarios chosen is done. The skin side is by far the most vulnerable area and large damages are predicted. The ice pressure largely exceed the stiffener capacity, and the skin plate fails prior to stabilization of the deformation field. Consequently, the global integrity of the structure is lost and flooding may lead to capsizing.

A collision at a height of 12 m, the lower column area, does not have a great influence on the hull beam strength because the stiffeners and plates resist some of the deformation. Plate deflection exceeding the critical limit would not happen if the assumptions in this thesis are assumed. Stiffener collapse may occur, but at a controlled extent. As for the possible reinforcements, actions should be taken to prevent both deck ice load and impacts in the pontoon-column intersection.

In previous work established by Kujala and Ehlers, one way of interpreting the repair costs is by letting costs be a function dependent on critical plastic deformation. No current criteria for the allowable indentation requiring repair exists. Results found in the current analysis show ice-induced indentations exceeding the suggested limit of 1/10 s, and repair actions are essential. The estimated increase of total weight from ice-strengthening is 1.5%, and repair costs from the design ice load are estimated to at least 6.2 mUSD.

It is noticed that the total weight increase is based on simplified assumptions. Preferably, skin stiffeners should withstand the majority of the pressure load so that all components are intact after a collision. This adds up to more required steel, and a correspondingly higher cost.

9.2 Further work

Based on the work in this thesis some recommendations for further work can be given. The different aspects are sorted in sections.

Geometry modelling

In this thesis, only the bow section is considered. The drilling rig as a whole can be modelled to investigate the total impact on the structure. A global model should be coarser meshed to keep the computation time at an acceptable level. Including the whole model means including mass and stability properties, and may affect the results found in the present thesis.

By analyzing only a local model, boundary conditions need to be introduced to represent the missing structure. This is making the structure behave relatively stiff and does not represent a fully realistic scenario. Detailed geometry of a larger part of the drilling rig can be made. These detailed parts should be modelled and meshing as to easily be included in the main model without significantly changing the computation time. However, a large detailed model will require larger computation time due to the increased number of elements, and should be considered when expanding the model.

Also, some detailed geometry is left out. This causes stress concentrations in for example corners to rise earlier than if the entire geometry is included. A full geometrical model of the CS60 can be created to eliminate these concentrations.

The mesh in the current model has been made from undistorted, four-node quad elements, but in sharp corners and other spots with advanced geometry, the elements are more distorted. Addressing and re-meshing these spots can be done to get more accurate results and to reduce the computation time.

Ice floe

An increasing pressure load is used to simulate the ice floe in this thesis. The pressure is applied to a pinned FE model, and the impact is evaluated. To get information about the actual collision of two moving bodies, a FE model of an ice floe may be made. As it is poor availability of both ice floe occurrence and physics, some simplifications and assumptions may be done to obtain a reasonable realistic model. An impact study with two impacting bodies may be done either using an initial velocity or a prescribed displacement approach.

Establishing a realistic model of an ice floe is seen to be difficult with respect to meshing and number of elements. Ph.D. Zhenhui Liu made a finite element iceberg model, [9], which may be used as a basis for an ice floe model.

Impact angle and area

The current analysis results describe the impact of a head on collision load. Other impact angles may be simulated to verify that the chosen impact yields reasonable results. By using existing models, the time spent on the analysis setup is limited.

In the present thesis, the contact area is assumed constant over frame and stiffener spacing. In a real ice impact, this will not be the case. Either by a finite element ice model or by pressure load, the increasing impact area should be taken into account.

Results

The procedure in [2] used a basis for the calculations assume plate strip theory. Other analysis methods considering entire plate fields may be implemented to verify the results given. More complex analysis may be carried out to capture other possible failure modes or reactions from the ice load. Also, hydrodynamic effects are not considered when analyzing local strength, and should be included in a global analysis.

Seen from a larger perspective, the suggested reinforcements may not be directly applicable to the current structure. Severe reinforcements are needed to design a complete ice-capable drilling rig, and the design process should be iterative to optimize as many factors as possible.

Bibliography

[1] Hagbart Skage Alsos. *Ship grounding - Analysis of ductile fracture, bottom damage and hull girder response*. Phd thesis, Norwegian University of Science and Technology, 2008.

[2] Jørgen Amdahl. Resistance of shuttle tanker m/t nordic torinita to ice impact. Technical report, Marintek, 2001.

[3] DNV. Structural design of column stabilised units (lrfd method). Recommended practice DNV-OS-C103, 2012.

[4] DNV. Ships for navigation in ice. Rules for classification of ships Part 5 Chapter 1, 2013.

[5] John O. Hallquist. LS-DYNA theory manual, March 2006.

[6] Heidi Jacobsen. Structural design considerations of an ice-resistance semi submersible drilling rig. Project thesis, Norwegian University of Science and Technology, December 2013.

[7] Pentti Kujala and Sören Ehlers. A risk-based evaluation ice-strengthened hull structures. In *ICETECH14*, 2014.

[8] H. Bruhns L. Zhang, E. D. Egge. Approval procedure concept for alternative arrangements. *Proceedings of the Third International Conference on the Collision and Grounding of Ships (ICCGS), Tokyo, Japan*, pages 87–97, 2004.

[9] Zhenhui Liu. *Analytical and numerical analysis of iceberg collisions with ship structures*. Phd thesis, Norwegian University of Science and Technology, 2011.

[10] Torgeir Moan. Chapter 8. Lecture notes in TMR4190 Finite Element Modelling and Analysis of Marine Structures, 2003.

[11] NORSOK. Design of steel structures. NORSOK Standard N-004, 2004.

[12] Egge Scharrer, Zhang. Abschlußbericht zum vorhaben mtk0614, kollisionsberechnungen in schiffbaulichen entwurfssystemen. Bericht Nr. ESS 2002.183, 2002.

[13] Martin Storheim. Analysis of structural damage of tankers subjected to collision. Master thesis, Norwegian University of Science and Technology, 2008.

[14] William James Stronge. *Impact Mechanics*. Press Syndicate of the University of Cambridge, 2000.

Appendix A

Excerpts from NORSOK Standard N-004 Annex A

The plastic analysis formulas used are shown in this appendix.

A.6.8.1 Elastic - rigid plastic relationships

In lieu of more accurate calculations rigid plastic theory combined with elastic theory may be used.

In the elastic range the stiffness and fundamental period of vibration of a clamped plate under uniform lateral pressure can be expressed as:

$r = k_1 w$ = resistance-displacement relationship for plate center

$k_1 = \psi \frac{D}{s^4}$ = plate stiffness

$T = \frac{2\pi}{\eta}\sqrt{\frac{\rho t s^4}{D}}$ = natural period of vibration

$D = E\frac{t^3}{12(1-\nu^2)}$ = plate bending stiffness

The factors ψ and η are given in Figure A.6-12

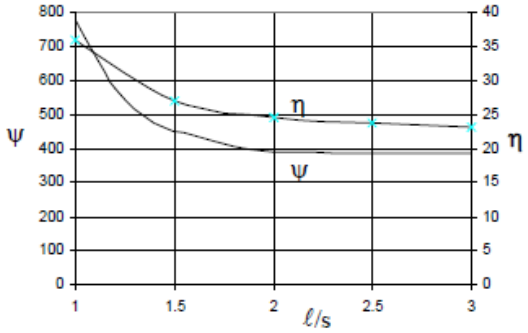

Figure A.6-12 Coefficients ψ and η

In the plastic range the resistance of plates subjected to uniform pressure can be taken as:

$$\frac{r}{r_c} = 1 + \overline{w}^2\left(\frac{\alpha + (3-2\alpha)^2}{9-3\alpha}\right) \qquad \overline{w} \le 1 \qquad \textbf{(A.6.8)}$$

$$\frac{r}{r_c} = 2\overline{w}\left(1 + \frac{\alpha(2-\alpha)}{3-\alpha}\left(\frac{1}{3\overline{w}^2} - 1\right)\right) \qquad \overline{w} \ge 1$$

Pinned ends :

$$\overline{w} = 2\frac{w}{t} \qquad r_c = \frac{6 f_y t^2}{\ell^2 \alpha^2}$$

Clamped ends :

$$\overline{w} = \frac{w}{t} \qquad r_c = \frac{12 f_y t^2}{\ell^2 \alpha^2}$$

$$\alpha = \frac{s}{\ell}\left(\sqrt{3 + \left(\frac{s}{\ell}\right)^2} - \frac{s}{\ell}\right) = \text{plate aspect parameter}$$

$\ell\,(>s)$ = plate length
s = plate width
t = plate thickness
r_c = plastic resistance in bending for plates with no axial restraint

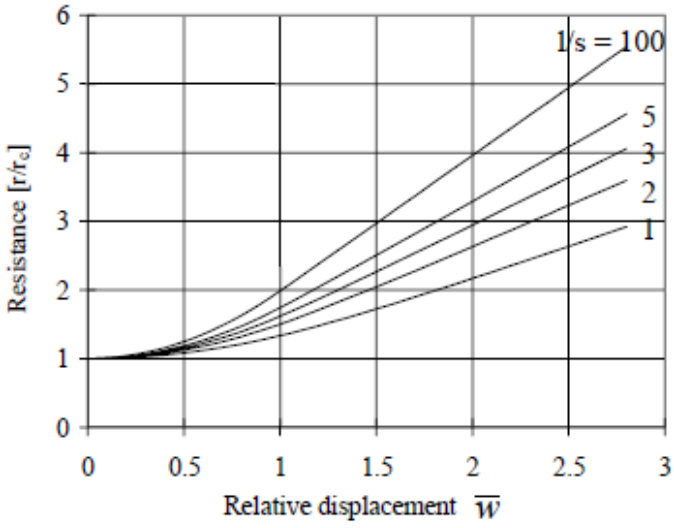

A.3.10.3 Tensile fracture

The degree of plastic deformation or critical strain at fracture will show a significant scatter and depends upon the following factors:

- material toughness;
- presence of defects;
- strain rate;
- presence of strain concentrations.

The critical strain for plastic deformations of sections containing defects need to be determined based on fracture mechanics methods, see 6.5. Welds normally contain defects and welded joints are likely to achieve lower toughness than the parent material. For these reasons structures that need to undergo large plastic deformations should be designed in such a way that the plastic straining takes place away outside the weld. In ordinary full penetration welds, the overmatching weld material will ensure that minimal plastic straining occurs in the welded joints even in cases with yielding of the gross cross section of the member. In such situations, the critical strain will be in the parent material and will be dependent upon the following parameters:

- stress gradients;
- dimensions of the cross section;
- presence of strain concentrations;
- material yield to tensile strength ratio;
- material ductility.

Simple plastic theory does not provide information on strains as such. Therefore, strain levels should be assessed by means of adequate analytic models of the strain distributions in the plastic zones or by non-linear finite element analysis with a sufficiently detailed mesh in the plastic zones.

When structures are designed so that yielding take place in the parent material, the following value for the critical average strain in axially loaded plate material may be used in conjunction with nonlinear finite element analysis or simple plastic analysis:

$$\varepsilon_{cr} = 0.02 + 0.65\frac{t}{\ell} \qquad \textbf{(A.3.22)}$$

where

t = plate thickness
ℓ = length of plastic zone (minimum 5t)

A.3.10.4 Tensile fracture in yield hinges

When the force deformation relationships for beams given in A.3.7.2 are used rupture may be assumed to occur when the deformation exceeds a value given by:

$$\frac{w}{d_c} = \frac{c_1}{2c_f}\left(\sqrt{1+\frac{4c_w c_f \varepsilon_{cr}}{c_1}} - 1\right) \qquad \textbf{(A.3.23)}$$

where the following factors are defined:

Displacement factor

$$c_w = \frac{1}{c_1}\left(c_{lp}\left(1-\frac{1}{3}c_{lp}\right)+4\left(1-\frac{W}{W_p}\right)\frac{\varepsilon_y}{\varepsilon_{cr}}\right)\left(\frac{\kappa\ell}{d_c}\right)^2 \quad \textbf{(A.3.24)}$$

plastic zone length factor

$$c_{lp} = \frac{\left(\frac{\varepsilon_{cr}}{\varepsilon_y}-1\right)\frac{W}{W_p}H}{\left(\frac{\varepsilon_{cr}}{\varepsilon_y}-1\right)\frac{W}{W_p}H+1} \quad \textbf{(A.3.25)}$$

axial flexibility factor

$$c_f = \left(\frac{\sqrt{c}}{1+\sqrt{c}}\right)^2 \quad \textbf{(A.3.26)}$$

non-dimensional plastic stiffness

$$H = \frac{E_p}{E} = \frac{1}{E}\left(\frac{f_{cr}-f_y}{\varepsilon_{cr}-\varepsilon_y}\right) \quad \textbf{(A.3.27)}$$

c_1	=	2	for clamped ends
	=	1	for pinned ends
c	=		non-dimensional spring stiffness, see A.3.7.2
κl	≤	$0.5l$	the smaller distance from location of collision load to adjacent joint
W	=		elastic section modulus
W_p	=		plastic section modulus
ε_{cr}	=		critical strain for rupture
$\varepsilon_y = \frac{f_y}{E}$			yield strain
f_y	=		yield strength
f_{cr}	=		strength corresponding to ε_{cr}

The characteristic dimension shall be taken as:

d_c	=	D	diameter of tubular beams
	=	$2h_w$	twice the web height for stiffened plates
	=	h	height of cross-section for symmetric I-profiles

For small axial restraint ($c < 0.05$) the critical deformation may be taken as

$$\frac{W}{d_c} = c_w\varepsilon_{cr} \quad \textbf{(A.3.28)}$$

The critical strain ε_{cr} and corresponding strength f_{cr} should be selected so that idealised bi-linear stress-strain relation gives reasonable results, see A.9. For typical steel material grades the following values are proposed:

Table A.3-4 Proposed values for e_{cr} and H for different steel grades

Steel grade	ε_{cr}	H
S 235	20 %	0.0022
S 355	15 %	0.0034
S 460	10 %	0.0034

Appendix B

Enclosed files

The relevant files for the calculation of plastic strength and FE model analysis are listed in this appendix. The mentioned files are delivered separately from this document.

- Ice_pressure_DNCOSC103.ods: Calculated ice pressure from Transit Rules.
- localmodel.key: Preliminary (damaged) MSc. Patran FE model implemented in LS PrePost with applied options.
- Pressurearea_and_loadcurve.ods: Impacted area plotted against resulting pressure force.
- Reinforcements_and_costs.ods: Applied reinforcements from original structure using procedure outlined in NORSOK N-004.
- Resistance_after_stiffener_collapse.ods: Calculation of resistance for plate field using procedure outlined in NORSOK N-004.
- Resistance_plates.ods: Calculation of resistance for stiffeners using procedure outlined in NORSOK N-004.
- Resistance_stiffeners.ods: Calculation of resistance for plate using procedure outlined in NORSOK N-004.
- Stress-strain_calibration.ods: Calibration of stress-strain relations using procedure outlined in Zhang, 2004.
- Tensile_fracture_in_yield_hinges.ods: Separate calculation of fracture using procedure outlined in NORSOK N-004.